J Porous Mater (2009) 16:409–418
DOI 10.1007/s10934-008-9213-z

New hydroxyapatite–hydrotalcite composites II. microwave irradiation effect on structure and texture

J. A. Rivera · G. Fetter · P. Bosch

Published online: 4 June 2008

Abstract Acid-basic materials are often used to catalyse organic reactions. Hydroxyapatite is acidic and hydrotalcite presents basic properties. The association of both compounds in a single material should present a rather unique catalytic behavior. Three preparations of hydroxyapatite impregnated with hydrotalcite are presented. The effect of microwave irradiation, at different preparation levels, is discussed. A homogeneous distribution of hydrotalcite on hydroxyapatite surface is obtained when hydrotalcite is precipitated over a previously microwave irradiated hydroxyapatite. Instead, if the hydrotalcite mixture is incorporated to the hydroxyapatite precursor gel and the resulting mixture microwave irradiated, hydrotalcite is preferentially deposited in the hydroxyapatite interparticle spaces. When both hydroxyapatite and hydrotalcite solutions are irradiated, mixed and irradiated again, the composite behaves as the addition of the two components.

Keywords Hydrotalcite · Hydroxyapatite · Composite · Microwave irradiation · Porous material · Bifunctional catalyst · Bone filling · Drug delivery · Phosphate · Hydroxide

J. A. Rivera · G. Fetter (✉)
Facultad de Ciencias Químicas, Universidad Autónoma de Puebla, Blvd. 18 Sur y Av. San Claudio, C.P. 72570, Puebla, PUE, Mexico
e-mail: geolarfetter@yahoo.com.mx

P. Bosch
Instituto de Investigaciones en Materiales, Universidad Nacional Autónoma de México, C.P. 04510, Mexico, DF, Mexico

1 Introduction

The synthesis of new composite materials hydrotalcite–hydroxyapatite provides acido-basic solids [1] whose features are due to the interaction of hydroxyapatite and hydrotalcite. They are both clays with different composition.

Hydrotalcites (HT) are double layered hydroxides whose chemical formula is:

$$[M^{2+}{}_{1-x}M^{3+}{}_{x}(OH)_2](A^{m-})_{x/m} \cdot nH_2O$$

where M^{2+} (which may be Mg, Ni, Zn) may be replaced by three-valent atoms, M^{3+} (normally Al, Fe) which produce positively charged layers. This charge is neutralized by A, a compensating anion with charge m^- asCO_3^{2-}, SO_4^{2-}, Cl^- or NO_3^-, among others; x represents the metal ratio $M^{3+}/(M^{3+} + M^{2+})$ and *n* the amount of crystallization water. The properties of hydrotalcite-like compounds are mainly determined by the metal ratio M^{2+}/M^{3+}, the concentration of the reactants in the synthesis solution and the synthesis procedure (hydrothermal, microwaves, ultrasound, sol–gel, pH value, among others) [2–4].

Their preference to carbonate ion as interlayer anion as well as their acid liability allow hydrotalcites to be compatible with a variety of biosystems like human being. These properties allow a variety of anionic substances (nucleotides, double stranded DNA, nucleic acid, vitamins, etc) to be intercalated into the interlayer space through electrostatic interaction [5]. They may remove as well fluoride from drinking water [6] and iodine from nuclear waste waters [7] or act as a solid basic catalyst [8].

The chemical formula of hydroxyapatite (HA) is:

$$M_{10}^{2+}(PO_4)_6(OH)_2$$

where M^{2+} is an exchangeable cation, usually calcium [9]. Hydroxyapatites have been used to anchor ruthenium complexes useful either in the Diels-Alder and aldolization reactions [10] or to support Ni–Mo sulphides [11]. Hydroxyapatites have found an extensive use for clinical applications as implants and coating due to their unique chemical composition and excellent biocompatibility with natural bones. Preparation of nanosized hydroxyapatite is an interesting target for technologies that involve restorative biomaterials. Nanometrical hydroxyapatite should mimic the particle size present in human body.

The performances of these two compounds in the same material, acid hydroxyapatite (cation exchanger) and basic hydrotalcite (anion exchanger), should depend on the interaction between the two compounds, determined through the preparation technique. The microwave irradiation during crystallization improves the preparation method. On the one hand, the crystallization time is significantly reduced, and, on the other, the precursor solutions may be more concentrated, allowing the use of smaller reactors [3, 4]. Furthermore, in a previous work [12] we have reported that the irradiation power determines the homogeneity of the obtained materials as at 600 W the obtained hydrotalcite is more homogeneous than the 200 W synthesis. As the irradiation power increases the particle size diminishes and the specific surface area increases. Hydroxyapatite has also been synthesized in presence of microwave irradiation with the same advantages, and nanorods, bowknot-like and flower-like nanomorphologies have been directly obtained [13–15]. If hydroxyapatite is prepared from gypsum in presence of microwave irradiation, gypsum powder can be completely converted to small hydroxyapatite crystals 0.03–0.3 μm long [16].

In a previous work [1], we reported that, in presence of microwave irradiation during the crystallization step of each compound, if the hydroxyapatite is first prepared, small hydrotalcite crystals are obtained. The scanning electron micrographs showed two particle morphologies, on the one hand, large particles similar to those reported for hydroxyapatite by other authors [17] and, on the other, small agglomerates growing in the intergranular spaces which correspond to hydrotalcite (grain size smaller than 1 μm). The specific surface area of this composite material was 143 m^2/g.

The interaction between hydrotalcite and hydroxyapatite should be enhanced if microwave irradiation is also used to obtain homogeneous precursor solutions. In this work, we have chosen to impregnate hydroxyapatite in three different ways. To understand the irradiation role, the samples are irradiated during different steps of the preparation. The microwave effect has to be, indeed, established.

2 Experimental

2.1 Hydroxyapatite synthesis

The hydroxyapatite sample was prepared from a 0.8 M H_3PO_4 (Baker) solution dropped in a 2 molar $Ca(OH)_2$ (Baker) solution at a constant pH of 9. The amount of reactants was such that the molar ratio Ca/P was equal to 1.67. The mixture was introduced in a microwave autoclave (MIC-I Sistemas y Equipos de Vidrio S.A. de C.V.) for 10 min. The used frequency, the power and the temperature were 2.45 GHz, 200 W and 80 °C. The resulting slurry is labeled slurry HA_{MW}. The sample was washed with deionized water until pH 10. Solids were recovered by decantation and dried in an oven at 70 °C (sample HA).

2.2 Hydrotalcite synthesis

The Mg/Al hydrotalcite-like sample was synthesized from two solutions: Mg- and Al-nitrate (Aldrich) water solution, 2.5 M and 2 M NaOH water solution. The flow of each solution was adjusted so that the pH was constant at 11.5. The amounts correspond to a molar ratio Mg/Al of 2. The resulting gel was treated in the microwave autoclave for 10 min operating at 2.45 GHz. The power was 200 W and the temperature was fixed at 80 °C. The resulting slurry is labeled slurry HT_{MW}. The solids were recovered by decantation and washed with distilled water up to a pH value of 10 and dried in an oven at 70 °C (sample HT).

2.3 Hydrotalcite incorporation to hydroxyapatite

(a) Hydrotalcite and hydroxyapatite were prepared as previously described and the resulting slurries were then mixed before microwave irradiation, maintaining the pH value, in both cases at 11.5. The mixture was then irradiated for 10 min as previously. The resulting sample, $(HT + HA)_{MW}$, was washed up to pH 10, recovered by decantation and dried at 70 °C. The nominal weight ratio hydrotalcite/hydroxyapatite was 1.

(b) The solution used to prepare hydrotalcite was used to impregnate the initially precipitated hydroxyapatite. The resulting mixture (slurry HT/HA) was submitted to microwave irradiation for 10 min as previously. The sample $(HT/HA)_{MW}$ was washed up to pH 10, recovered by decantation and dried at 70 °C. The nominal weight ratio hydrotalcite/hydroxyapatite was 1.

(c) The solution used to prepare hydrotalcite was used to impregnate the initially precipitated and irradiated hydroxyapatite (slurry HA_{MW}). The resulting mixture (slurry HT/HA_{MW}) was submitted to microwave irradiation for 10 min as previously. The sample $(HT/HA_{MW})_{MW}$ was washed up to pH 10, recovered by

decantation and dried at 70 °C. The nominal weight ratio hydrotalcite/hydroxyapatite was 1. The sequence of the three mixed preparations is summarized in Scheme 1.

2.4 Characterization

2.4.1 X-ray diffraction

A Bruker-axs D8-advance diffractometer coupled to a copper anode X-ray tube was used to identify the compounds present in the powdered samples. A diffracted beam monochromator selected the Kα radiation.

2.4.2 FTIR spectroscopy

FTIR spectra in the region 4,000–400 cm^{-1} were obtained with a Magna-IR Spectrometer 550 Nicolet. The pellets were prepared with KBr.

2.4.3 Nitrogen adsorption

The BET surface areas were determined by the conventional multipoint technique with a Micromeritics ASAP 2020. The pore size distribution curves were obtained by the BJH method. The samples were pretreated at 200 °C for 10 h at high vacuum.

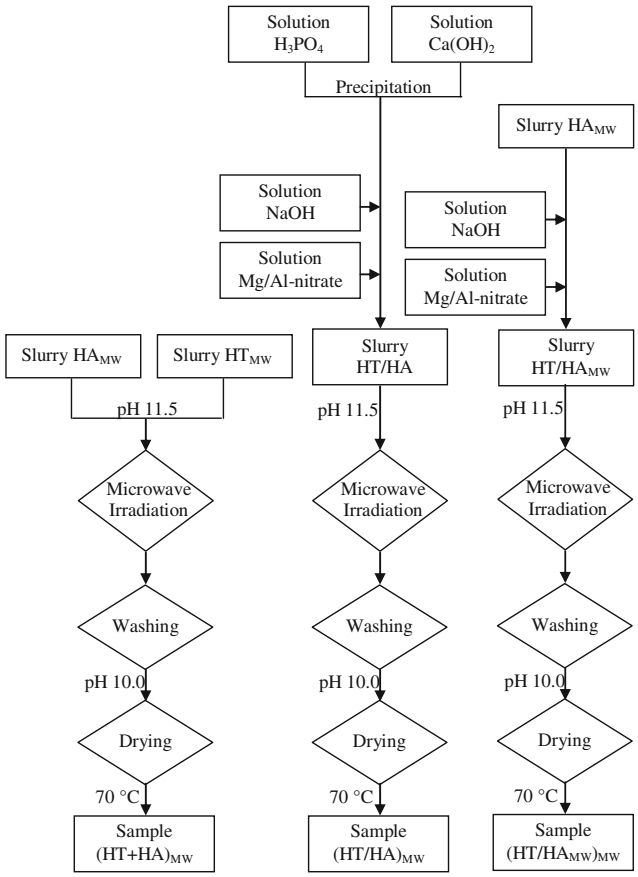

Scheme 1 Representation of the composites synthesis processes

2.4.4 Scanning electron microscopy

A scanning electron microscope LEICA, Stereoscan 440 was used. The samples were previously covered with gold to avoid charge problems. Using the EDS detector a mapping of a selected zone of the sample $(HT + HA)_{MW}$ was obtained for calcium and magnesium, as these elements are characteristic of hydroxyapatite and hydrotalcite, respectively.

2.4.5 Chloride ion adsorption

Chloride content of each residual solution was analyzed at 25 °C with a potentiometer coupled to an electrode Mettler Toledo ISE Combination Chloride. Then the chloride amount in the corresponding sample was estimated by difference.

3 Results

3.1 Compounds

Figure 1 compares the X-ray diffraction patterns of the hydrotalcite and the hydroxyapatite obtained; they correspond to well crystallized compounds and no impurities are observed in the X-ray diffraction limits (more than 3%).

In all the diffractograms of the composite materials, hydrotalcite and hydroxyapatite were identified, Fig. 2. Indeed, although the hydrotalcite 003 peak appears at the same angle (2θ) as the very small 100 peak of hydroxyapatite, the hydrotalcite presence can be established as the relative intensity increases noticeably. If the sample is prepared as a mixture which is then irradiated, sample $(HT + HA)_{MW}$, the corresponding peaks of each compound are well defined and intense, showing that both compounds are constituted by large independent crystals. Then, hydrotalcite layers are well ordered and the corresponding 003 peak appears at 11.5° (2θ) [18]. The pattern corresponding to the hydrotalcite solutions incorporated to precipitated hydroxyapatite and, then, irradiated, $(HT/HA)_{MW}$ sample, presents well defined hydroxyapatite peaks typical of a crystalline compound. Note that the hydroxyapatite 200 peak located at $2\theta = 21.8°$ in the sample $(HT + HA)_{MW}$ is now found at $2\theta = 20.0°$. The interplanar distance in this direction is, then, larger. The hydrotalcite peaks are broader than those observed in the previous sample, thus microwave irradiation alters selectively, in this case, the crystallite size of hydrotalcite or introduces strains between planes. In the third preparation, $(HT/HA_{MW})_{MW}$ sample, the peaks of both

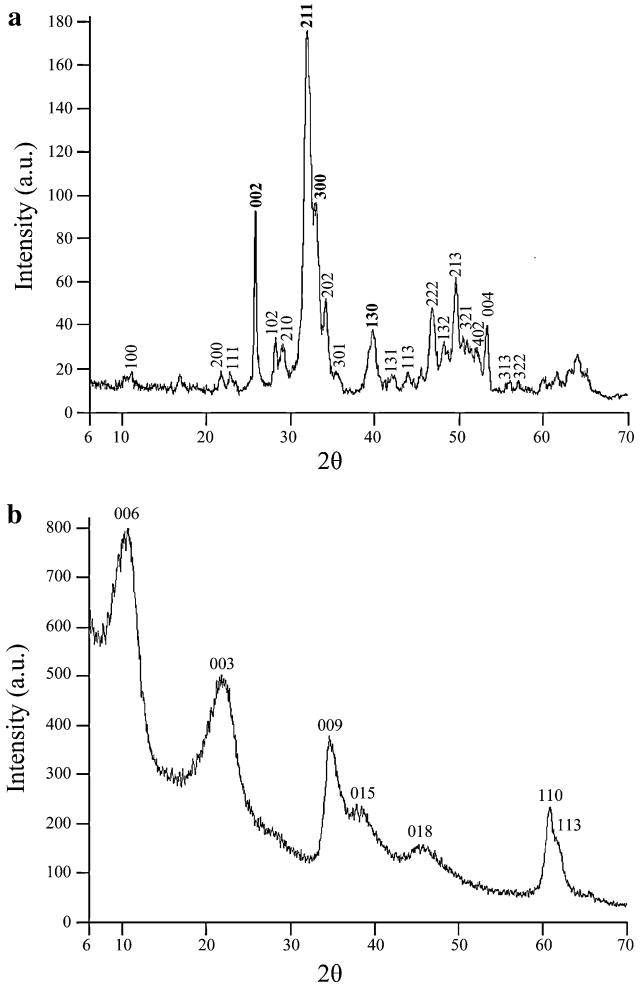

Fig. 1 X-ray diffraction patterns of the hydroxyapatite (**a**) and the hydrotalcite (**b**) samples

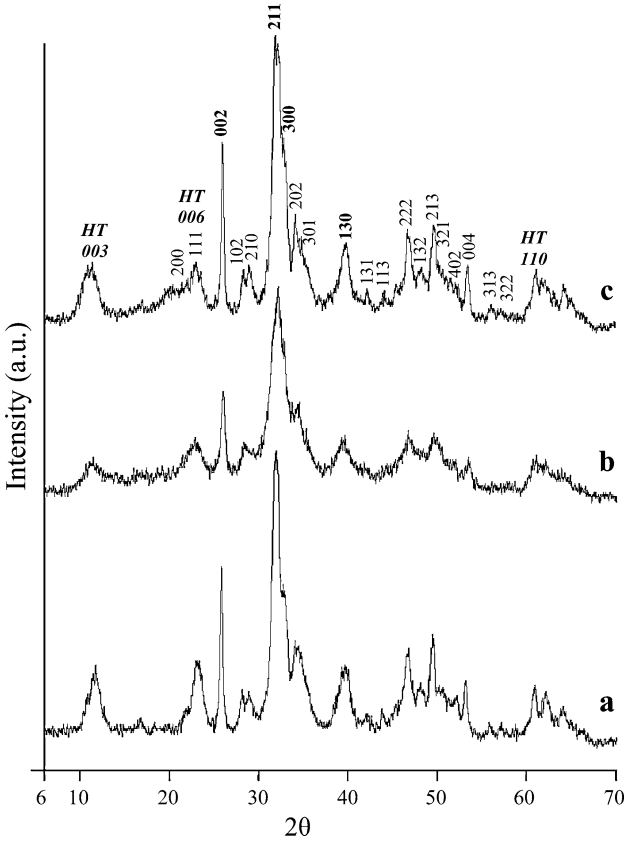

Fig. 2 X-ray diffraction patterns of the composites $(HT + HA)_{MW}$ (**a**), $(HT//HA_{MW})_{MW}$ (**b**) and $(HT/HA)_{MW}$ (**c**)

compounds, hydrotalcite and hydroxyapatite, are broad. The pattern presents a higher background line which can be assigned to a higher content of a microcrystalline compound. Hence, small and defective crystals of hydroxyapatite and hydrotalcite as well as small particles not detected by X-ray diffraction should be present.

3.2 Species

Figure 3 shows the hydroxyapatite and hydrotalcite infrared spectra, they both present bands at ca. 3,450 and 1,640 cm^{-1} due to hydroxyl radicals. The two compounds can be differentiated through bands at 1,387 cm^{-1} in hydrotalcite and the doublet at 1,097 and 1,038 cm^{-1} in hydroxyapatite. All the infrared spectra of the composite materials present the typical bands (1,097 and 1,038 cm^{-1}) of hydroxyapatite and of hydrotalcite (1,387 cm^{-1}). Still, in the $(HT/HA)_{MW}$ sample, the intensity of the 1,387 cm^{-1} band, due to interlayered nitrates in hydrotalcites [19], diminishes significantly. Then, hydrotalcite most probably is formed with the phosphates dissolved from the hydroxyapatite during the microwave treatment. The profile of the pattern is similar to that of pure hydroxyapatite excepting the small hydrotalcite peak at 1,381 cm^{-1}.

3.3 Morphology

The morphology of the synthesized hydroxyapatite and hydrotalcite is different enough to distinguish them, as hydrotalcite presents a constant particle size (0.5 μm) and faceted morphology, Fig. 4. In some regions the lamellar structure is clearly observed. Instead, hydroxyapatite distribution is broad (1–30 μm) and the particle shape is globular. Nevertheless, both compounds seem to be formed by small associated entities.

The composite material morphology can be interpreted in terms of the observed hydroxyapatite or hydrotalcite. The sample $(HT + HA)_{MW}$ has a two modal size distribution as smooth particles larger than 20 μm appear with smaller ones of ca. 1 μm, Fig. 5. The sizes, as well as the appearance, correspond to hydroxyapatite and hydrotalcite, respectively. To confirm such attribution a Mg- and Ca-mapping is presented in Fig. 6, as calcium is unique to

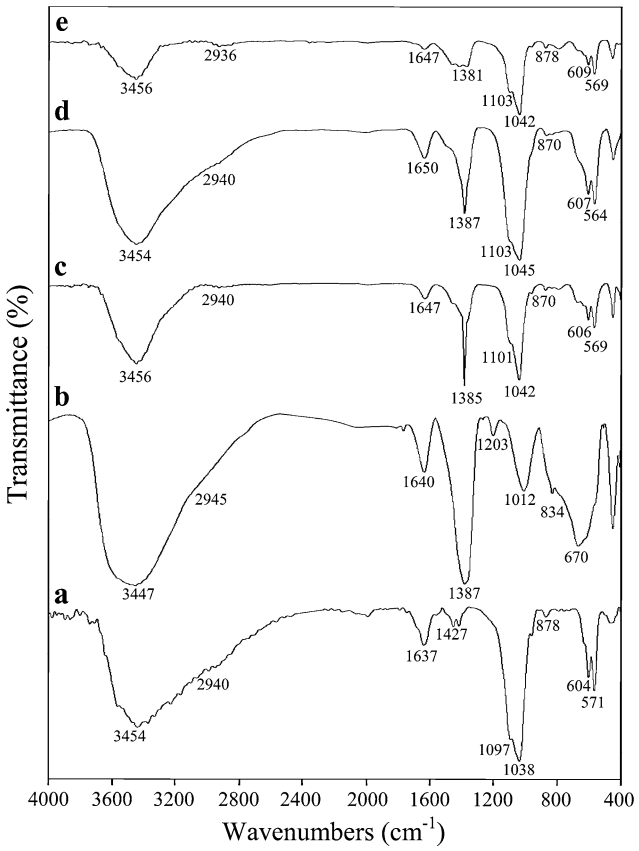

Fig. 3 Infrared spectra of the HA (**a**), HT (**b**), $(HT + HA)_{MW}$ (**c**), $(HT/HA_{MW})_{MW}$ (**d**) and $(HT/HA)_{MW}$ (**e**) samples

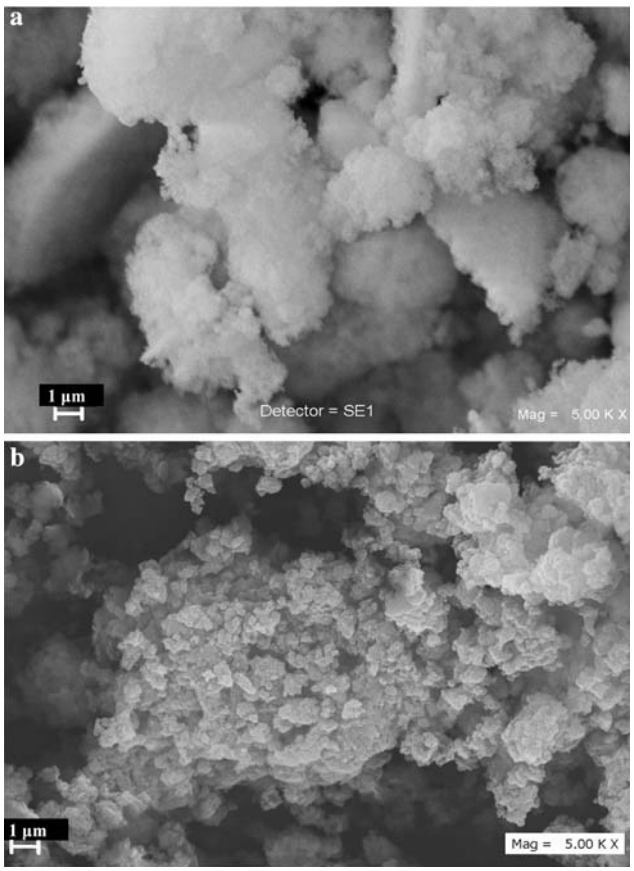

Fig. 4 Scanning electron micrographs of the HA (**a**) and the HT (**b**) samples

hydroxyapatite and Mg to hydrotalcite. The large chunks are calcium enriched, thus they are hydroxyapatite, whereas the small particles, as they present magnesium, must be hydrotalcite. This sample seems to be a mixture of the two compounds.

Instead, sample $(HT/HA_{MW})_{MW}$ is very homogeneous, Fig. 7. Particles are all 0.2 µm. They are distributed in large clusters of ca. 10 µm. Hence, it seems that hydroxyapatite is covered by small crystallites of hydrotalcite as no large smooth chunks are observed.

The $(HT/HA)_{MW}$ is the most complex composite, Fig. 8. Large bricks of 7–10 µm presenting smooth surfaces are found together with smaller lamellar particles in the inter-particle spaces. It seems that the small particles are hydrotalcite and the large ones are hydroxyapatite.

Then, depending on the microwave treatment the hydrotalcite distributes on the hydroxyapatite in different locations. The strongest interaction is obtained in the $(HT/HA_{MW})_{MW}$ sample.

3.4 Surface areas

Table 1 reports the surface areas of each compound. The hydrotalcite area is larger than that of the hydroxyapatite, as expected. When hydrotalcite is synthesized on hydroxyapatite the surface areas are much larger. The sample $(HT + HA)_{MW}$ has a surface area of 170 m^2/g. This value is much higher than any of the areas obtained for the non composite materials. The deposition of hydrotalcite on hydroxyapatite with a final microwave irradiation seems to disperse the hydrotalcite. Indeed the X-ray diffraction patterns as the micrographs show that hydroxyapatite is formed by very large particles. But, if the irradiation is applied first to the hydroxyapatite precursor solution and then to the mixture, sample $(HT/HA_{MW})_{MW}$, the surface area is 204 m^2/g, showing that hydrotalcite particles are very small, as already suggested by the SEM images. The $(HT/HA)_{MW}$ has an area 50% lower (100 m^2/g). As shown by IR results, this sample contains probably interlayered phosphates. Again the hydrotalcite particles are very small although they are located in the hydroxyapatite inter-particle spaces. The difference between this sample and the previous one is the hydroxyapatite precursor solution irradiation. Then, this factor seems to be crucial in order to obtain a good interaction between hydroxyapatite and hydrotalcite surfaces and, therefore, a large surface area.

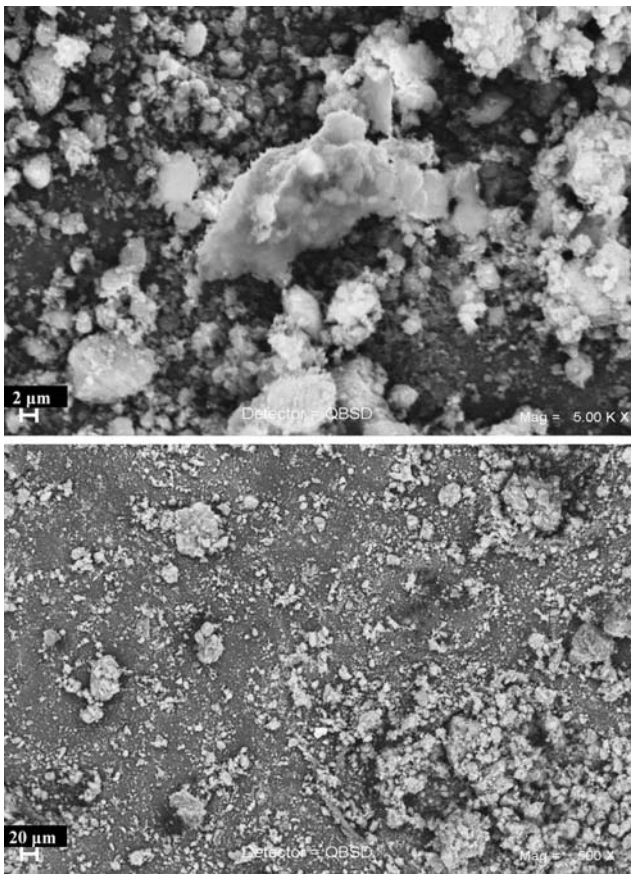

Fig. 5 Scanning electron micrographs of the $(HT + HA)_{MW}$ sample

3.5 Pore size distribution

The pore size distribution of hydroxyapatite presents a maximum at d = 33 Å, the curve indicates also the presence of large pores up to 300 Å, Fig. 9. The hydrotalcite pore size distribution is monomodal, centered at 34 Å, the curve decreases up to 300 Å. The composite material $(HT + HA)_{MW}$ has a broad pore size distribution from 20 to 540 Å, the maximum is at 105 Å. Sample $(HT/HA_{MW})_{MW}$ has a broad distribution which comprises diameters from 20 to 540 Å, and it presents a peak at 34 Å. The composite $(HT/HA)_{MW}$ pore size distribution is trimodal and less broad. The maxima are at 31, 90 and 140 Å, lastly the distribution goes down to 300 Å. The interaction between hydrotalcite and hydroxyapatite, depending on the irradiation treatment, determines the porosity of the resulting material as irradiation distributes the location and the interaction of hydrotalcite among the hydroxyapatite particles.

3.6 Chloride sorption

In Fig. 10, the performance of HA and HT in chloride retention differs, after 90 min, in ca. 22 ppm/g (i.e. 50%).

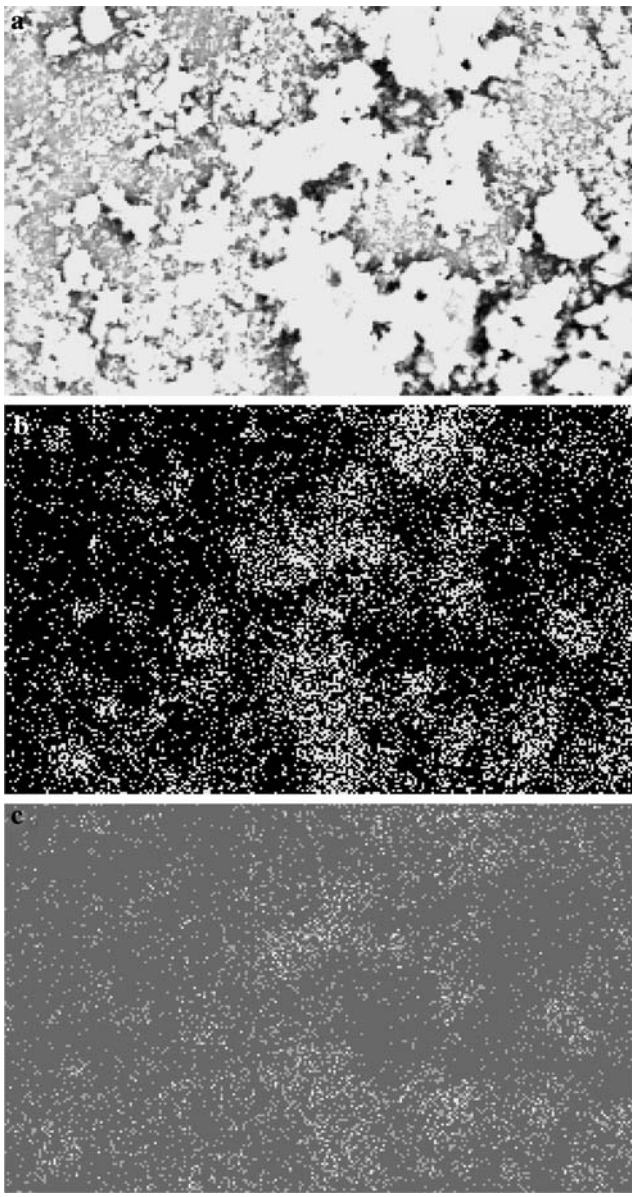

Fig. 6 Local composition of the sample $(HT + HA)_{MW}$: SEM image (**a**), Ca-map (**b**) and Mg-map (**c**)

In hydroxyapatite, hydroxyls are easily exchanged by chlorides. In hydrotalcite the retention mechanism is either due to an ion exchange or to sorption on the hydrotalcite defects. A hypothetical mechanical mixture 1–1 of the two synthesized HA and HT compounds would adsorb after 90 min 38 ppm/g. This amount is indeed retained by the $(HT/HA)_{MW}$ sample within error range, it is most interesting as, for chloride retention, the interlayered anion (nitrate or phosphate) in hydrotalcite is not determinant. The sample $(HT + HA)_{MW}$ retains the same amount of chloride as HT. Last, but not least, the sample $(HT/HA_{MW})_{MW}$ improves the chloride sorption of pure HA, then, the chloride retention sequence can be:

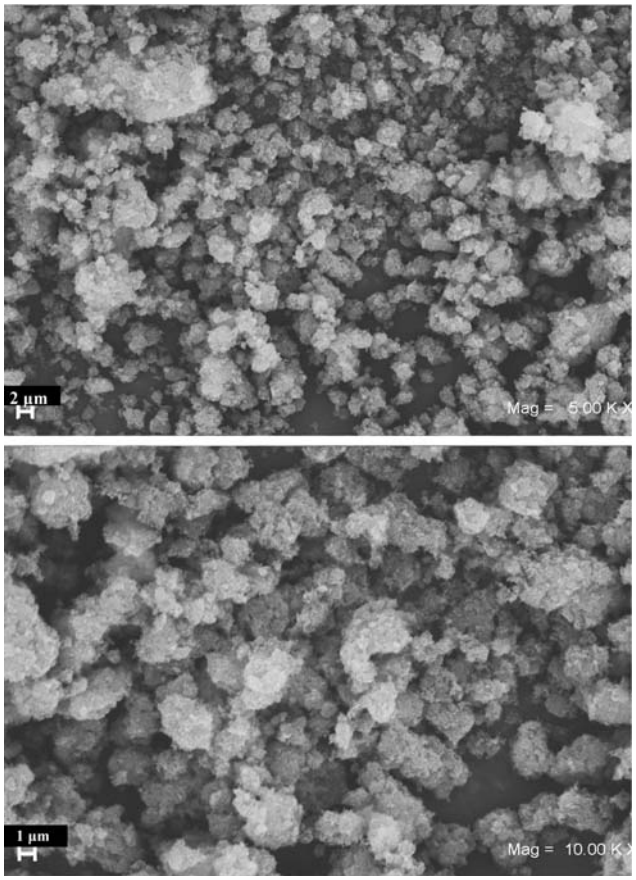

Fig. 7 Scanning electron micrographs of the $(HT/HA_{MW})_{MW}$ sample

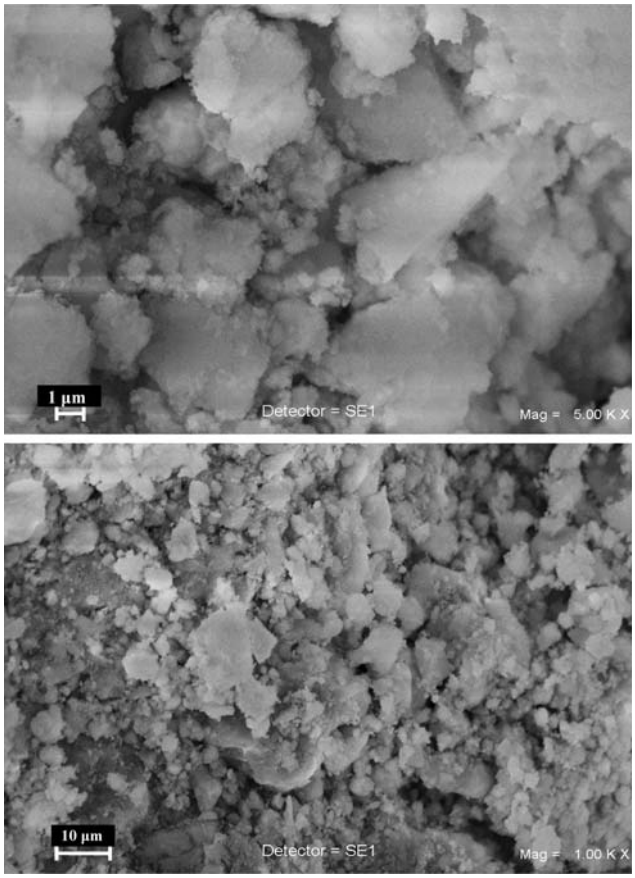

Fig. 8 Scanning electron micrographs of the $(HT/HA)_{MW}$ sample

$$HT = (HT + HA)_{MW} < (HT/HA)_{MW} < HA < (HT/HA_{MW})_{MW}$$

4 Discussion

The results may be summarized as follows. The microwave irradiation of the hydroxyapatite solution, $(HT/HA_{MW})_{MW}$ sample, provides composites where the interaction between hydrotalcite and hydroxyapatite is strong. Instead, the two other preparations (irradiation after hydrotalcite and hydroxyapatite precursors mixture or irradiation of hydroxyapatite before impregnation with irradiated hydrotalcite) behave as a mixture although the hydrotalcite in the second protocol is located in the interstitial space between hydroxyapatite particles.

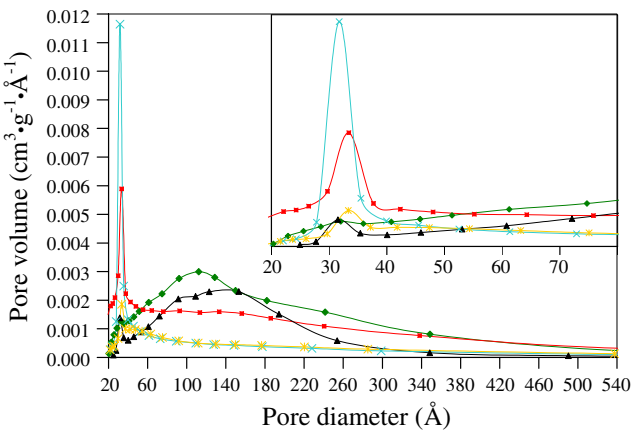

Fig. 9 Pore size distributions of the samples: HA ( ), HT ( ), $(HT + HA)_{MW}$ ( ), $(HT/HA_{MW})_{MW}$ ( ) and $(HT/HA)_{MW}$ ( ) samples

Table 1 Surface area of the samples

Sample	HA	HT	$(HT + HA)_{MW}$	$(HT/HA_{MW})_{MW}$	$(HT/HA)_{MW}$
Surface area (m^2/g)	66	89	170	204	100

Hydroxyapatite powders have been synthesized in presence of surfactants to reduce the particle size which diminished from 0.1 to 0.05 μm [19, 20]. Temperature and pH of hydrothermal synthesis are crucial on the morphology of hydroxyapatite [21]. When microwave irradiation is used [13], it is found that the pH value and the complex reagent EDTA determine hydroxyapatite nanorods, bowknot-like and flower like nanostructures whose size is ca.1 μm. In our conditions (pH 11.5 and no complex reagent), microwave irradiation provided a globular HA with a 1–30 μm particle size.

In hydrotalcite synthesis the particle size was homogeneous (0.5 μm) and reproduces the values reported in the bibliography [22–24]. Hence, microwave irradiation in the crystallization step does not seem to alter the hydrotalcite morphology.

The composite material $(HT + HA)_{MW}$ is synthesized irradiating the mixture of the previously microwave irradiated hydroxyapatite and hydrotalcite slurries. The hydroxyapatite particle size, in this sample, was larger than 20 μm, this size is much larger than the hydrotalcite particle diameter (1 μm). This sample turns out to be a simple mixture of the two components, no strong interaction between them can be determined.

In this sense the sample $(HT/HA)_{MW}$ is more complex as the 200 hydroxyapatite peak was shifted towards smaller angles. In this sample, as the solutions are not irradiated, nitrate anions may diffuse slowly into the hydroxyapatite structure substituting hydroxyls as in fluorapatites. Hydroxyapatite crystals are smaller (7–10 μm) than those of sample $(HT + HA)_{MW}$. Hydrotalcite crystallizes in the interparticle spaces as it crystallizes first due to its solubility constant [25].

In the $(HT/HA_{MW})_{MW}$ sample, as the hydroxyapatite solution was first microwave irradiated, and then, the hydrotalcite precursor solutions added, the dispersion of hydrotalcite precursors should be very homogeneous and the amount of Mg cations should be very high. This is the main

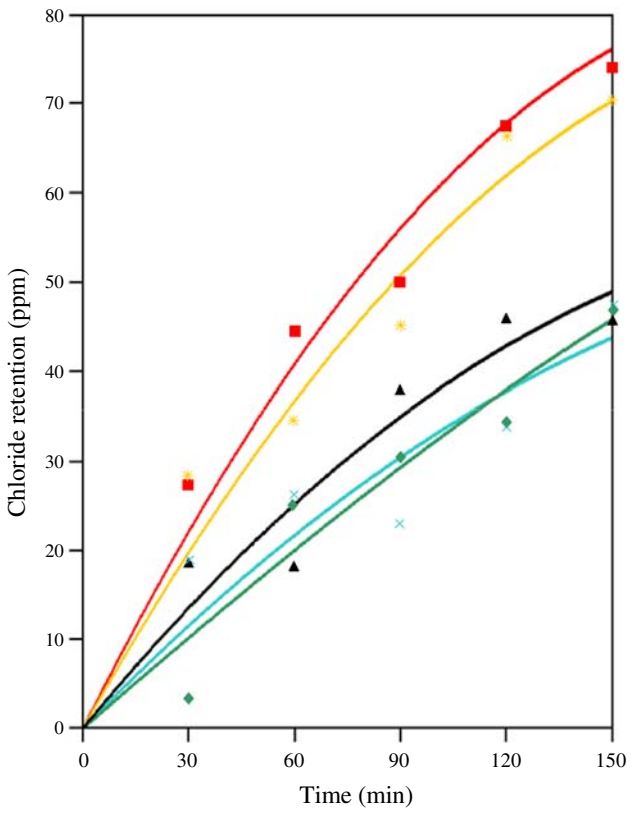

Fig. 10 Chloride adsorption isotherms of the samples: HA ( ), HT ( ), $(HT + HA)_{MW}$ ( ), $(HT/HA_{MW})_{MW}$ ( ) and $(HT/HA)_{MW}$ ( ) samples

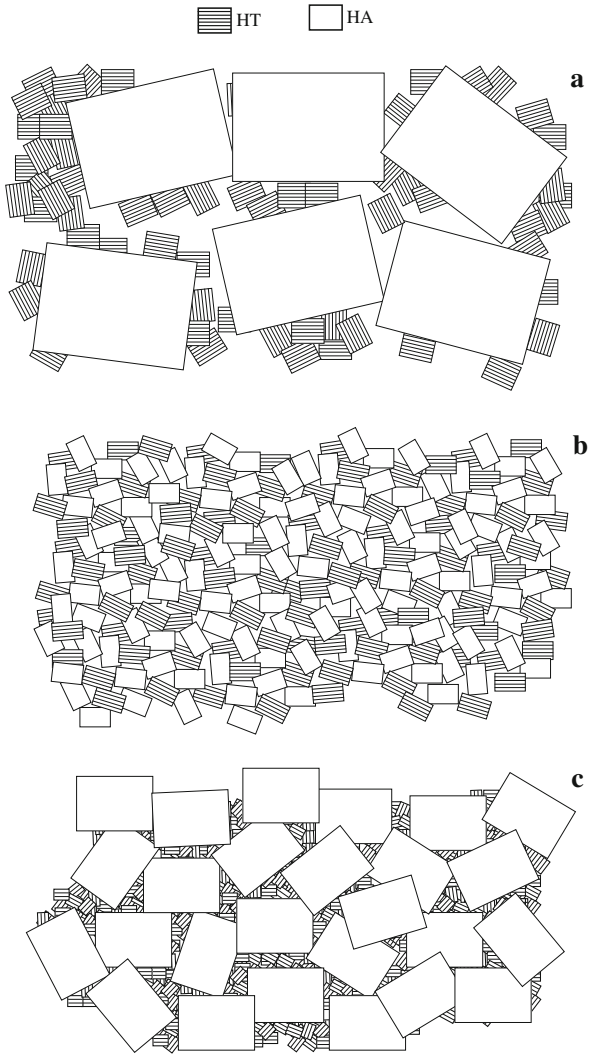

Scheme 2 Structural assembling representation of the composites: $(HT + HA)_{MW}$ (**a**), $(HT/HA)_{MW}$ (**b**) and $(HT/HA_{MW})_{MW}$ (**c**)

difference between the previous preparations and the present synthesis. In this case the hydrotalcite is no more located in the interparticle spaces, it is regularly distributed on the hydroxyapatite surface interacting strongly as shown by the surface area results and chloride sorption. Furthermore, the pore size distribution may be explained as the composition of the hydrotalcite pore size distribution (peak at 34 Å) and a larger porosity (from 60 to 540 Å) corresponding to the assembly of the two compounds. Hydrotalcite, then, grow over the hydroxyapatite surface in the shape of desert roses through Mg atoms and edge hydroxides on hydroxyapatite surface. Such structure may be understood if the Mg^{2+} role is considered. The hydrotalcite slurry is rich in this cation, which may poison hydroxyapatite crystal surface [25] and block further growth. Magnesium ions are in contact with the hydroxyapatite seeds. Hydrotalcite limits hydroxyapatite crystal growth.

Chloride retention can be explained following the previous considerations. Indeed, two samples, $(HT + HA)_{MW}$ and $(HT/HA)_{MW}$ reproduce the behavior of the single components, the first one is similar to HT and the second one to HA. Therefore, the adsorbing material, i.e., the compound accessible to chloride must be HT in $(HT + HA)_{MW}$ and the other way round for $(HT/HA)_{MW}$. Our proposition is represented in Scheme 2 where in $(HT + HA)_{MW}$ the large hydroxyapatite particles are practically covered by hydrotalcite which inhibits chloride access to hydroxyapatite. Instead, in $(HT/HA)_{MW}$ sample the hydrotalcite agglomerates are occlude into the hydroxyapatite crystals, chloride is almost only retained by this compound. Sample $(HT/HA_{MW})_{MW}$ is constituted by a mixture of both hydroxyapatite and hydrotalcite whose crystal sizes are smaller. As the surface area is higher the material is less compact, chloride anions may access simultaneously to both compound surfaces.

5 Conclusion

Microwave irradiation tailors the distribution of hydrotalcite over hydroxyapatite. If the hydrotalcite solution is used to impregnate the previously synthesized hydroxyapatite, $(HT/HA_{MW})_{MW}$, the resulting composite hydrotalcite-hydroxyapatite is constituted by a regular distribution of hydrotalcite and small hydroxyapatite particles and the interaction between these two compounds may be strong. Instead, if the hydrotalcite solution is added to a non irradiated hydroxyapatite, $(HT/HA)_{MW}$, the hydrotalcite crystallizes selectively in the hydroxyapatite interparticle spaces forming large crystalline agglomerates. When the two microwave irradiated slurries (hydrotalcite and hydroxyapatite) were mixed and, then, irradiated again, $(HT + HA)_{MW}$, hydroxyapatite forms large crystals and hydrotalcite is deposited on top. Chloride sorption performance was determined by such morphologies.

Such structures determine the probable use of the hydroxyapatite–hydrotalcite composite materials. For instance, as hydrotalcite is a well known drug dispenser, the hydroxyapatite bone filling function could be complemented by the in situ delivery process of the exchanged hydrotalcite. Such composites could be useful in biomedicine. In catalysis, many processes are based on a two-step acid and basic mechanism. Our composites associate both functions in a single material. The catalytic reactions should proceed differently in the three presented samples as the distribution of hydrotalcite and hydroxyapatite should condition the proximity of acid (hydroxyapatite) and basic (hydrotalcite) sites.

Acknowledgements The authors gratefully acknowledge the financial support of CONACYT and the technical work of L. Baños and J. Guzmán.

References

1. J.A. Rivera, G. Fetter, P. Bosch, in *Proceedings of the XX Simp. Iberoamer. Catal.*, (Gramado, Brasil, 2006)
2. J. He, M. Wei, B. Li, Y. Kang, D.G. Evans, X. Duan, Struct. Bond. **119**, 89 (2006)
3. J. Olanrewaju, B.L. Newalkar, C. Mancino, S. Komarneni, Mater. Lett. **45**, 307 (2000)
4. J.A. Rivera, G. Fetter, Y. Jiménez, M.M. Xochipa, P. Bosch, Appl. Catal. A **316**, 207 (2007)
5. F. Li, X. Duan, Struct. Bond. **119**, 193 (2006)
6. H. Wang, J. Chen, Y. Cai, J. Ji, L. Liu, H.H. Teng, Appl. Clay Sci. **35**, 59 (2007)
7. G. Fetter, M.T. Olguín, P. Bosch, S. Bulbulian, J. Porous Mater. **7**, 469 (2000)
8. B.F. Sels, D.E. de Vos, P.A Jacobs, Catal. Rev. **43**, 443 (2001)
9. S. Chakraborty, S. Bag, S. Pal, A.K. Mukherjee, J. Appl. Cryst. **39**, 385 (2006)
10. K. Mori, T. Hara, T. Mizugaki, K. Ebitani, K. Kaneda, J. Am. Chem. Soc. **125**, 11460 (2003)
11. N. Elazarifi, M.A. Chaoui, A.E. Ouassouli, A. Ezzamarty, A. Travert, J. Leglise, L.C. de Ménorval, C. Moreau, Catal. Today **98**, 161 (2004)
12. J.A. Rivera, G. Fetter, P. Bosch, Microporous Mesoporous Mater. **89**, 306 (2006)
13. J. Liu, K. Li, H. Wang, M. Zhu, H. Yan, Chem. Phys. Lett. **396**, 429 (2004)
14. S. Meejoo, W. Maneeprakorn, P. Winotai, Thermochim. Acta **447**, 115 (2006)
15. A. Siddharthan, S.K. Seshadri, T.S. Sampath Kumar, Scr. Mater. **55**, 175 (2006)
16. H. Katsuki, S. Furuta, J. Am. Ceram. Soc. **82**, 2257 (1999)
17. W. Bonfield, M. Wang, K.E. Tanner, Acta Mater. **46**, 2509 (1998)
18. F. Cavani, F. Trifiro, A. Vaccari, Catal. Today **11**, 173 (1991)
19. Y. Wang, J. Chen, K. Wei, S. Zang, X. Wang, Mater. Lett. **60**, 3227 (2006)
20. W.J. Shih, M.C. Wang, M.H. Hon, J. Cryst. Growth **275**, e2339 (2005)
21. J. Liu, K. Li, H. Wang, M. Zhu, H. Xu, H. Yan, Nanotechnology **16**, 82 (2005)

22. T. Lopez, P. Bosch, E. Ramos, R. Gómez, O. Navarro, D. Acosta, F. Figueras, Langmuir **12**, 189 (1996)
23. N. Iyi, T. Matsumoto, Y. Kaneko, K. Kitamura, Chem. Mater. **16**, 2926 (2004)
24. S. Vial, V. Prevot, C. Forano, J. Phys. Chem. Solids **67**, 1048 (2006)
25. F.C.M. Driessens, R.M.H. Verbeeck, in *Biominerals*, (CRC Press, 1990), p. 91